Cell

Structure of the Autoinhibited Kinase Domain of CaMKII and SAXS Analysis of the Holoenzyme

Oren S. Rosenberg,[1,2,3,5] Sebastian Deindl,[1,2,3] Rou-Jia Sung,[1,2,3] Angus C. Nairn,[6] and John Kuriyan[1,2,3,4,*]

[1] Department of Molecular and Cell Biology
[2] Department of Chemistry
[3] Howard Hughes Medical Institute
University of California, Berkeley, Berkeley, CA 94720, USA
[4] Physical Biosciences Division, Lawrence Berkeley National Lab, Berkeley, CA 94720, USA
[5] Department of Cell Biology
[6] Department of Psychiatry
Yale University School of Medicine, New Haven, CT 06508, USA
*Contact: kuriyan@berkeley.edu

SUMMARY

Ca^{2+}/calmodulin-dependent protein kinase-II (CaMKII) is unique among protein kinases for its dodecameric assembly and its complex response to Ca^{2+}. The crystal structure of the autoinhibited kinase domain of CaMKII, determined at 1.8 Å resolution, reveals an unexpected dimeric organization in which the calmodulin-responsive regulatory segments form a coiled-coil strut that blocks peptide and ATP binding to the otherwise intrinsically active kinase domains. A threonine residue in the regulatory segment, which when phosphorylated renders CaMKII calmodulin independent, is held apart from the catalytic sites by the organization of the dimer. This ensures a strict Ca^{2+} dependence for initial activation. The structure of the kinase dimer, when combined with small-angle X-ray scattering data for the holoenzyme, suggests that inactive CaMKII forms tightly packed autoinhibited assemblies that convert upon activation into clusters of loosely tethered and independent kinase domains.

INTRODUCTION

Calcium/calmodulin (Ca^{2+}/CaM)-dependent protein kinase II (CaMKII) is one of the most important transducers of Ca^{2+} signals in a variety of cell types and is highly conserved across animal species (Hudmon and Schulman, 2002). A fundamental difference between CaMKII, which assembles into a dodecameric holoenzyme, and other CaM-dependent kinases is that CaMKII has the capacity to retain a "memory" of prior activation by Ca^{2+}/CaM because of a two step activation process. In the first step, which is similar to the activation process of the monomeric CaM kinases (Goldberg et al., 1996; Hu et al., 1994; Mayans et al., 1998), Ca^{2+}/CaM removes an autoinhibitory regulatory segment located C-terminal to the kinase domain (Figure 1A). This releases the catalytic activity of the enzyme and makes accessible a regulatory residue, Thr 286 (mouse CaMKIIα isoform numbering, used throughout the text). The second step is the phosphorylation of Thr 286 by another kinase domain within the oligomeric holoenzyme (Lai et al., 1986; Lou and Schulman, 1989; Miller et al., 1988; Rich and Schulman, 1998; Schworer et al., 1988; Thiel et al., 1988). Phosphorylation of Thr 286 keeps CaMKII active in the absence of Ca^{2+}/CaM by preventing the rebinding of the regulatory segment to the kinase domain (Lai et al., 1986; Miller and Kennedy, 1986; Yang and Schulman, 1999) and by increasing the affinity of CaM for the enzyme by ~13,000-fold (Meyer et al., 1992). Regulated activation (Lisman et al., 2002) and deactivation (Nelson et al., 2005) of the enzymatic activity have both been shown to be important to the physiological function of CaMKII.

C-terminal to the autoinhibitory segment in CaMKII is the "association domain," which assembles CaMKII into a dodecameric holoenzyme (Gaertner et al., 2004; Morris and Torok, 2001; Woodgett et al., 1983). Once a kinase subunit is activated by Ca^{2+}/CaM, it can phosphorylate adjacent subunits that are also bound to Ca^{2+}/CaM. If the concentration of Ca^{2+} is high, phosphorylation on Thr 286 will spread rapidly through the holoenzyme, leading to the onset of Ca^{2+}/CaM-independent activity. When the Ca^{2+} concentration is low, Thr 286 is dephosphorylated before activation can proceed. Little is known at present about how the structure of the holoenzyme controls the acquisition of Ca^{2+}/CaM autonomous activity. Also poorly understood is how the architecture of the holoenzyme prevents the high local
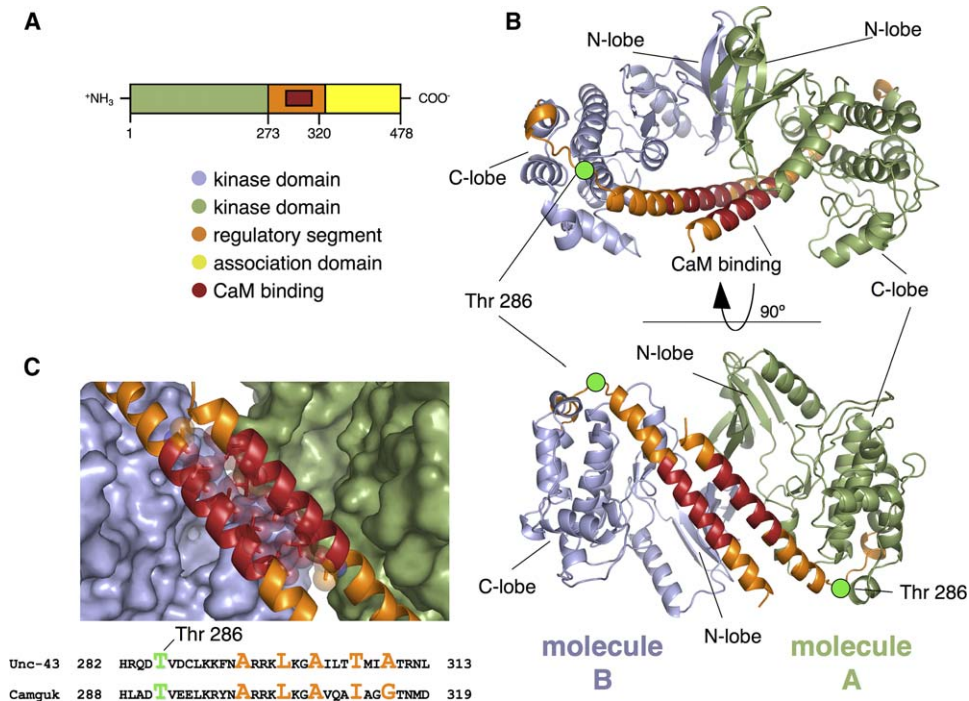
Figure 1. The Crystal Structure of the Autoinhibited Kinase Domain of CaMKII

(A) The domain organization of CaMKII.

(B) Two views of the CaMKII dimer, 90° rotated from each other. Molecule A is shown in green and molecule B is shown in blue. The Ca^{2+}/CaM binding residues are shown in magenta and the rest of the regulatory segment is shown in orange.

(C) Detailed view of the coiled-coil region of the dimer. Shown in spheres are the residues at the interface in a "knobs and holes" packing. Residues at the interface of the coiled coil highlighted in orange. These include the regulatory residue Thr 306 (Colbran, 1993). Also shown is the homologous region of the *Drosophila* protein Camguk that binds to the residues involved in the coiled coil of CaMKII (Lu et al., 2003) suggesting that other proteins may exploit these residues to form similar coiled-coil structures.

concentration of kinase domains from generating background phosphorylation levels that would interfere with the proper response to Ca^{2+}.

The crystal structure of the association domain of mouse CaMKIIα has been determined and reveals a stacked arrangement of two 7-fold symmetric rings (Hoelz et al., 2003). The formation of 14-membered rather than the expected dodecameric rings by the isolated association domain is a consequence of removing the kinase domains (O.S.R., S.D., L. Comolli, A. Hoelz, K. Downing, A.C.N., and J.K., unpublished data). The fundamental unit of assembly is a dimer of association domains, consisting of one subunit each from the upper and lower rings. The N-terminal segments of each association domain form α helices that are arrayed around the edges of the midplane of the assembly and serve as the connection points for the kinase domains. A model for the dodecameric association-domain ring can be generated by removing one dimeric element from the 14-membered ring and closing the gap while maintaining symmetry (Hoelz et al., 2003; O.S.R., S.D., L. Comolli, A. Hoelz, K. Downing, A.C.N., and J.K., unpublished data).
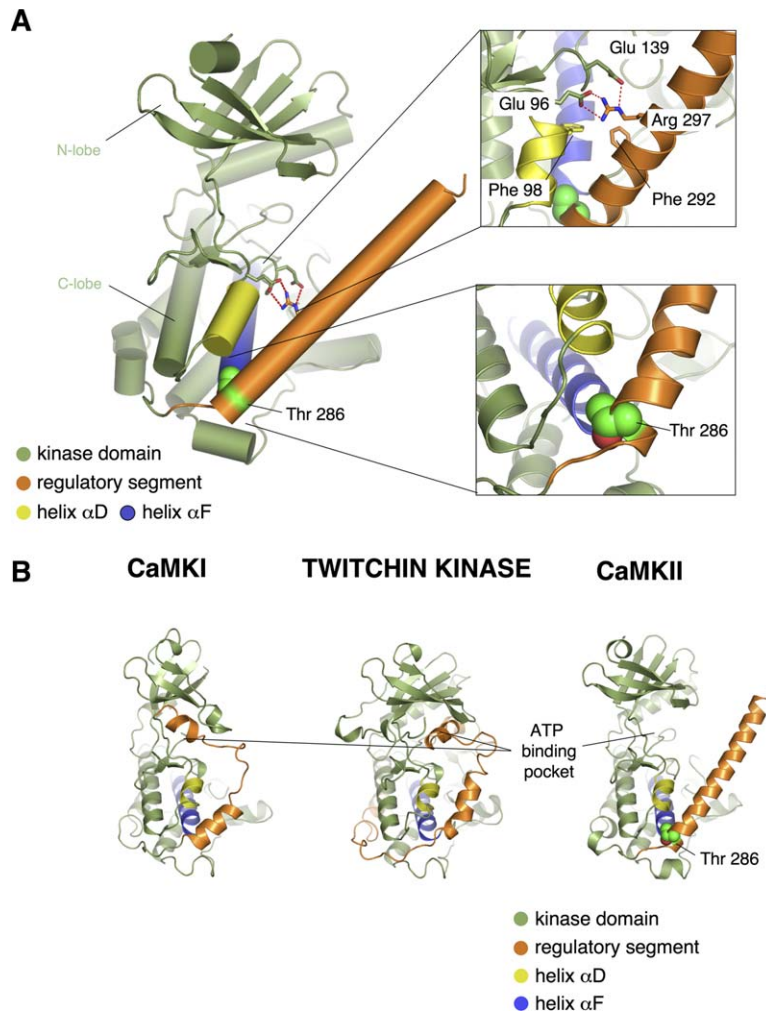
We describe here the crystal structure of the autoinhibited kinase domain of CaMKII and discuss how it is maintained in an inactive state by the Ca^{2+}/CaM responsive regulatory element. An unexpected feature of the structure is the organi-zation of the autoinhibited kinase domains into dimers, in a manner that is suggestive of a mechanism for controlling autophosphorylation within the holoenzyme. Small-angle X-ray scattering (SAXS) analysis suggests that the auto-inhibited and dimeric kinase domains are arranged in a ring that is coplanar with and tightly packed against the ring formed by the association domain. Arrangement of the kinase domains in this manner has important consequences for the mechanism by which CaMKII is activated and acquires Ca^{2+}/CaM-independent activity.

RESULTS AND DISCUSSION

The Regulatory Segments of CaMKII Form a Dimeric Coiled-Coil Structure

We crystallized the kinase and regulatory domains (residues 1–340, referred to in this text as "the autoinhibited kinase domain") of *Caenorhabditis elegans* CaMKII, UNC-43 (all *C. elegans* constructs described here were derived from the splice variant K11E8.d) The use of an inactive mutant enzyme (Asp 135 Asn) was required for prevention of heterogeneity due to phosphorylation (data not shown). This fragment of *C. elegans* CaMKII is 77% identical in sequence to the corresponding region of human CaMKIIα (see Figure S1 in the Supplemental Data available with this article online). There

A

- ● kinase domain
- ● regulatory segment
- ● helix αD ● helix αF

B   CaMKI   TWITCHIN KINASE   CaMKII

- ● kinase domain
- ● regulatory segment
- ● helix αD
- ● helix αF

Figure 2. Details of the Interaction between the Kinase Domain and the Regulatory Segment

(A) Detailed view of the interactions between the regulatory segment and the main body of the kinase domains. In the top panel, the substrate binding residues Glu 96 and Glu 139 (Yang and Schulman, 1999) are shown interacting with Arg 297 from the regulatory segment. The bottom panel shows the regulatory Thr 286 sitting at the C-terminal end of helix αF. Mutation of residues Phe 98 in helix αD and Phe 292 in the regulatory segment activate the kinase strongly (Yang and Schulman, 1999).

(B) Comparison of three Ca^{2+}/CaM-activated kinases, CaMKI (Goldberg et al., 1996), twitchin kinase (Hu et al., 1994), and CaMKII. In CaMKII, neither the N lobe nor the ATP binding pocket make any contact with the regulatory segment.

are two structurally similar autoinhibited kinase domains in the asymmetric unit of the crystal (Table S1; Experimental Procedures).

The regulatory segment (residues 273–317) emerges from the base of the kinase domain and runs, at its N-terminal end, through the channel formed between helices αD and αF of the kinase (Figures 1 and 2). It ends in a long α helix. The regulatory segment separates from the main body of the kinase at residue Arg 297, at which point it begins to make hydrophobic interactions with the regulatory helix from the other kinase domain in the asymmetric unit. The CaM binding residues span residues 290 to 314 within the regulatory segment (Figures 1B and 1C; see also Meador et al. [1993]).

The two regulatory helices form a left-handed and antiparallel coiled coil, ending at residue 315 (Crick, 1953; Walshaw and Woolfson, 2001). The region between residues 291 and 320 of CaMKII is predicted to form a coiled coil with a low but significant probability (Lupas et al., 1991). In contrast, the monomeric CaM-dependent kinases show little or no probability of coiled-coil formation in the regulatory segment (Figure S2).

Gel filtration and analytical ultracentrifugation experiments demonstrate that the autoinhibited kinase domain is mono-

meric in solution at concentrations below ~100 μM (data not shown). Electron microscopic images of the most expanded forms of CaMKII correspond to a cylinder of radius ~100 Å and height ~200 Å (Kolodziej et al., 2000). Using these dimensions, the local concentration of subunits is estimated to be in the range of 3 mM within the holoenzyme. The two elements of the coiled coil are linked to spatially adjacent points on the association domain, which is likely to further strengthen their interaction. At the same time, the coiled coil cannot be so strong that the binding of Ca^{2+}/CaM to it is impeded. It is therefore not surprising that the isolated autoinhibited kinase domains are monomeric at low concentration rather than dimeric.

In order to determine whether the autoinhibited kinase domains interact with one another within the holoenzyme, we compared the binding of fluorescent Ca^{2+}/CaM to C. elegans CaMKII holoenzyme (Asp 135 Asn mutant) and to an isolated autoinhibited kinase domain fragment. The CaMKII holoenzyme binds to Ca^{2+}/CaM with an EC_{50} value of 145 nM (±12) and with an apparent Hill coefficient of 2.3 (±0.4) (Figure S3). These values are similar to those presented previously for mammalian CaMKII (Gaertner et al.,
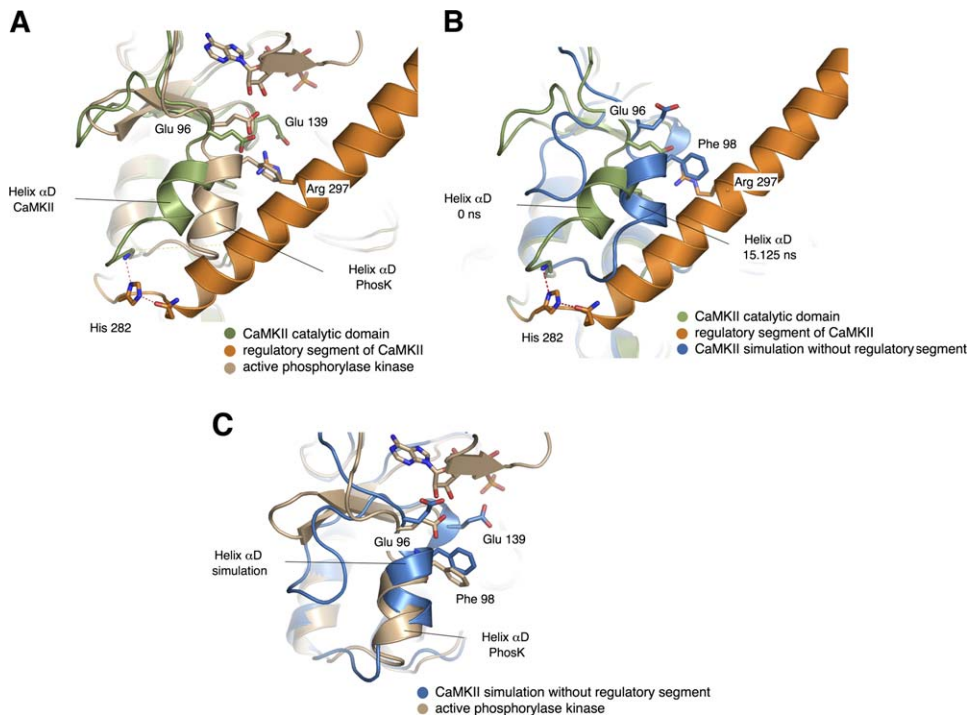
Figure 3. An Allosteric Mechanism Affecting the ATP Binding Site

(A) A structural alignment of phosphorylase kinase (PhosK, bound to ATP; Lowe et al., 1997) and CaMKII showing the rotation and translation of helix αD and the interactions of His 282. Note the position of Glu 96 in CaMKII, in a location too distant to interact with ATP. All residue numbering refers to CaMKII.

(B and C) After ~15 ns of molecular-dynamics simulation without the regulatory segment, helix αD rotates spontaneously into the position seen in PhosK.

(B) An overlay of the crystal structure of CaMKII (inactive) with an instantaneous structure, at 15.125 ns, from the simulation without the regulatory segment.

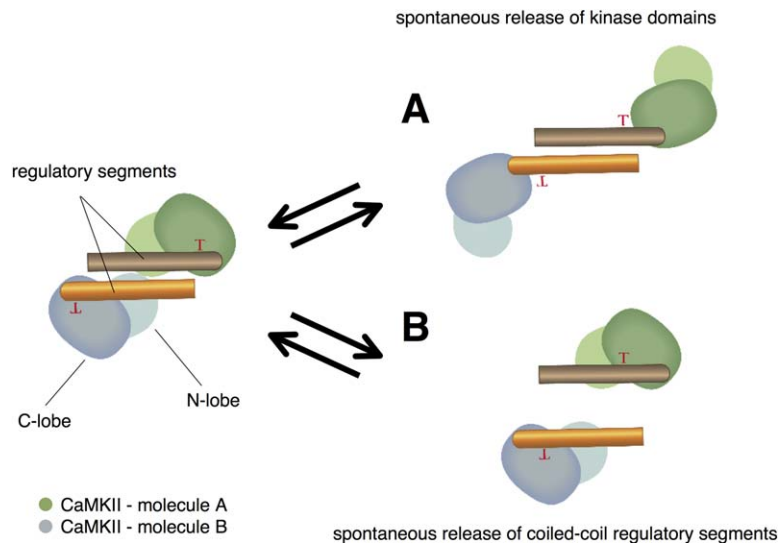(C) The same 15.125 ns instantaneous structure, at 15.125 ns, overlaid with PhosK (active).

2004). In contrast, the binding of the isolated autoinhibited kinase domain (Asp 135 Asn mutant) to Ca^{2+}/CaM occurs with an EC_{50} value of 40 nM ± 18 and an apparent Hill coefficient of 1.2 ± 0.4.

Although these data do not directly confirm that the particular dimer we see in the crystal structure is relevant for holoenzyme function, the Hill coefficient of ~2 for Ca^{2+}/CaM binding to the holoenzyme is consistent with a sequential binding model in which the first Ca^{2+}/CaM to bind to the holoenzyme disrupts a higher-order structure, thereby facilitating the binding of a second Ca^{2+}/CaM molecule. Taken together with the evidence that the autoregulatory domains form a classical coiled coil it is reasonable to hypothesize that the interactions we see in the crystal structure of the autoinhibited kinase domain are similar to those that exist in the holoenzyme.

The Kinase Domain of CaMKII Is Intrinsically Active but Is Held in an Autoinhibited State

CaMKII does not require phosphorylation for catalytic activity, and the structure of the autoinhibited kinase domain of CaMKII displays many hallmarks of active protein kinases (Nolen et al., 2004; Figure S4A). Nevertheless, the kinase is held in an inactive state by the regulatory segment, which blocks substrate binding (Figure 2).

The affinity of ATP for CaMKII is reduced significantly in the absence of Ca^{2+}/CaM (Colbran, 1993; Hanson and Schulman, 1992; King et al., 1988; Shields et al., 1984). It is surprising, therefore, to find that the regulatory segment of CaMKII avoids the ATP binding site of the N lobe of the kinase. This contrasts with the close interactions seen between the regulatory segment and the ATP binding site in monomeric CaM kinases (Figure 2B). The reduced ATP affinity of autoinhibited CaMKII could be due to a significant change in the orientation of helix αD in the C lobe of the kinase (Figure 3A), which is rotated by 45° and translated by 5 Å with respect to its orientation in active phosphorylase kinase, a closely related CaM-activated kinase (Lowe et al., 1997). In active kinases, a residue corresponding to Glu 96 in CaMKII coordinates the hydroxyl groups of the ribose ring of ATP (Huang et al., 1995; Lowe et al., 1997). In CaMKII, the regulatory segment causes the rotation of helix αD, which swings Glu 96 away from the ATP binding site. His 282 forms a hydrogen bond with the amide nitrogen in the backbone of Tyr 108 and anchors the D helix in its inactive state (Figure 3A). Mutation of His 282 has been shown experimentally to alter ATP binding to CaMKII (Brickey et al., 1994; Smith et al., 1992). ATP binding to CaMKII may also be weakened by an ~15° outward rotation in the relative orientations of the N and C lobes of the kinase domain that is stabilized by the formation of a network of ionic

spontaneous release of kinase domains

regulatory segments

N-lobe

C-lobe

● CaMKII - molecule A
● CaMKII - molecule B

spontaneous release of coiled-coil regulatory segments

Figure 4. The Coiled-Coil Strut Is Part of a Mechanism Preventing Autophosphorylation

This schematic diagram illustrates the consequences of structural fluctuations that release either the kinase domains or the coiled-coil interaction.

If kinase domains prematurely release from the regulatory segment in the absence of Ca^{2+}/CaM as shown in (A), the coiled-coil strut will prevent the active site from interacting with the regulatory Thr 286. If, as shown in (B), the coiled-coil interaction breaks, the interactions with the regulatory segment will also prevent accidental phosphorylation of Thr 286.

interactions among residues Glu 17, Arg 28, and Glu 38 in the dimer (Figure S4B).

The altered orientation of helix αD has been seen in other inactive CaM kinases (Goldberg et al., 1996; Hu et al., 1994), but structures of both the active and inactive states of the kinase domain are not available for any one member of the CaMK family. We therefore analyzed the consequences of removing the regulatory segment on the orientation of helix αD by using molecular dynamics simulations. Four simulations were generated: one each for the dimer unit and a monomer with the regulatory segment, and two for the kinase-domain monomer without the regulatory segment. Each of these trajectories was calculated for a fully solvated protein using periodic boundary conditions and the program AMBER (Case et al., 2004, University of California, San Francisco) and extends to 9.0 ns, 16.5 ns, 20.0 ns, and 39.2 ns, respectively.

As expected, in the dimer structure and in the monomer with the regulatory domain in place there were no gross changes in the overall conformation. Strikingly, in both of the simulations with the regulatory segment removed, the orientation of helix αD changed after ∼10 ns in one simulation and after ∼30 ns in the other simulation so that it more closely resembled the conformation seen in active kinases. Glu 96 can now interact readily with the hydroxyl groups of the ribose of ATP (Figures 3B, 3C, and S5). This spontaneous transition into the active conformation suggests that removal of the constraints imposed by the regulatory segment would lead to the ready acquisition of catalytic activity by the kinase domain.

The Critical Phosphorylation Site (Thr 286) Is Held Apart from the Active Sites by the Coiled-Coil Strut

Thr 286, the phosphorylation of which renders the enzyme Ca^{2+}/CaM independent, is buried between the surface of the αD/αF channel and the regulatory segment. The threonine side chain is located almost precisely at the negative pole of the helix dipole of helix αF (Figure 2A), and phosphor-

ylation will clearly destabilize the docking of Thr 286 in the αD/αF channel.

There is a clear spatial separation between the region of the regulatory segment involved in inhibiting the kinase domain (residues 280 to 295 on one face of the helix) and the region that forms the coiled-coil interaction (residues 293 to 317 on the other face of the helix). This implies that a transient release of the regulatory segment from the αD/αF channel of the kinase domain can occur with retention of the coiled-coil interaction, which serves as a strut to keep the two active sites away from either of the Thr 286 sites of phosphorylation (Figure 4A). Likewise, a spontaneous disruption of the coiled-coil interaction would still have the regulatory segment bound to the kinase domain (Figure 4B). Transautophosphorylation would require the simultaneous breakage of the coiled-coil interaction and the release of the autoinhibitory segments from both kinase domains, which appears much less likely without the addition of Ca^{2+}/CaM.

Analysis of Holoenzyme Structure using Small-Angle X-Ray Scattering (SAXS)

Two quite different models have been proposed, based on electron microscopy, to describe the assembly of the CaMKII holoenzyme (Kolodziej et al., 2000; Morris and Torok, 2001). In one model the kinase domains are arranged in a plane around the central ring of the association domain, forming a flattened disc (Morris and Torok, 2001). In the other model the holoenzyme is roughly cylindrical with a height of ∼200 Å, and the kinase domains are located above and below the plane of the association-domain ring in an alternating pattern such that they do not interact (Kolodziej et al., 2000).

In order to distinguish between these two models, we made a series of SAXS measurements for full-length *C. elegans* CaMKII and compared the results to the predicted scattering from a set of model dodecameric holoenzyme structures. The radius of gyration (R_g) of the holoenzyme was determined to be 72 Å from our SAXS data. Six dimeric autoinhibited kinase domains were arrayed around the central

ring of a dodecameric association domain, modeled on the basis of the crystal structure (Hoelz et al., 2003). Calculations of the R_g of the holoenzyme model are very sensitive to changes in the distance from the center of the association-domain ring to the centers of mass of the autoinhibited kinase domains. We fixed the radial position of the kinase dimer (in the plane of the association domain) at a distance that resulted in a calculated R_g value that is closest to the experimental value. This model places the kinase dimers such that they pack against the α helices extending from the association domain (Figure 5A; see also Figure 7A for a cartoon rendering).

Examination of maps of electrostatic surfaces of the association domain and of the autoinhibited kinase-domain dimer reveals a striking complementarity between the edges of the association-domain disk and the regulatory segments of the kinase domains (Figures S6A and S6B). We rotated the autoinhibited kinase domain dimers so as to align their surfaces based on the electrostatic complementarity. The calculated R_g values are not very sensitive to rotations of the kinase dimer around axes that are parallel to the midplane of the association-domain ring. Thus, this rotational placement is not constrained significantly by the SAXS data and should simply be considered as a reasonable juxtaposition of the two assemblies.

Starting from this model, each kinase dimer was then separated into individual kinase domains arrayed symmetrically in planes above and below the midplane. By varying the vertical separation of the kinase-domain rings, a series of structural models was generated (Figures 5A and 5B). The radius of gyration of each model in the series was calculated using the program package Crysol (Svergun et al., 1995) and compared to the experimental value of R_g (72 Å). As the autoinhibited kinase domains move out of the plane of the association domain, the calculated values of R_g deviate sharply from the experimental value (Figure 5C).

We also generated a series of models that had the same calculated value of R_g (matching the experimental value for the *C. elegans* holoenzyme) by displacing the rings of the autoinhibited kinase domains above and below the association domains while simultaneously shrinking the radius of the autoinhibited kinase rings (Figure 5D). The fit of the calculated scattering curve to the experimental curve was found to be best for a model in which the individual autoinhibited kinase domains are held together as dimer pairs in an outer ring that is coplanar with the central plane (Figures 5E and 5F).

In the next step of the SAXS analysis, we generated shape reconstructions for the holoenzyme using a simulated annealing procedure (Svergun, 1999). Based on earlier electron microscopic data showing 6-fold symmetry in the holoenzyme (Morris and Torok, 2001) and crystallographic data showing a 2-fold symmetry in the association domain (Hoelz et al., 2003), we imposed a constraint of 622 symmetry on the reconstruction of the shape of the holoenzyme. The final shape reconstruction (see Experimental Procedures) is a flattened disk with a diameter of ∼200 Å and a height of ∼60 Å (Figures 6A and 6B).

The reconstruction has a hole in its center with a diameter of ∼20 Å, and the 6-fold symmetric model of the association domain can be readily docked into the reconstruction so that it wraps around the hole. Arranged around this central core of the shape reconstruction are six protrusions that extend out parallel to the plane of the association-domain ring. We interpret these protuberances as general indications of the positions of the kinase-/regulatory-domain dimers and have docked the holoenzyme model (described above and shown in Figure 6B) into the SAXS shape reconstruction. As the C lobes of the kinases are mainly helical and expected to be more rigid, we speculate that the six stalks arrayed from the central association-domain ring represent two adjacent C lobes, with the intervening weaker features in the shape reconstruction corresponding to pairs of adjacent N lobes. This alternating pattern of electron density is compatible with the two-dimensional reconstructions of Morris and Torok (2001).

We have checked the robustness of these results by carrying out shape reconstructions with 32 symmetry (one 3-fold axis with perpendicular 2-fold axes) instead of 622 symmetry (Figure S7A). We also did a SAXS-based shape reconstruction for the *M. musculus* CaMKIIα holoenzyme (Figure S7B) that was generally very similar to that of the *C. elegans* holoenzyme. As a further control, we also carried out a shape reconstruction for the mouse CaMKIIα association domain (residues 334–472), for which the crystal structure is known (Hoelz et al., 2003). The shape reconstruction, obtained without imposing any constraints of symmetry, shows satisfactory agreement with the crystal structure (Figure S7C).

Speculation Regarding Holoenzyme Activation

One of the most intriguing properties of CaMKII is its ability to respond to Ca^{2+} signals in a manner that depends on the frequency with which Ca^{2+} levels rise and fall (De Koninck and Schulman, 1998). When the frequency of Ca^{2+} pulses is low, the kinase activity of CaMKII directly tracks the concentration of Ca^{2+}. When the frequency of Ca^{2+} pulses is increased, there is a remarkable change in the behavior of the enzyme, and it acquires constitutive activity due to transautophosphorylation on Thr 286 (Hudmon and Schulman, 2002).

Transautophosphorylation of Thr 286, which occurs within one holoenzyme, requires both the phosphorylating kinase subunit and the "substrate" kinase subunit to be bound to Ca^{+2}/CaM (Bradshaw et al., 2002; Hanson et al., 1994; Rich and Schulman, 1998). In order for the holoenzyme to be sensitive to the frequency and not just the amplitude of Ca^{2+} pulses, there has to be a delay between the first activation event (the binding of Ca^{2+}/CaM to one regulatory segment) and the activation of a second kinase domain (Hudmon and Schulman, 2002). Schulman and coworkers have posited that this delay arises from the greater probability of the second activation event occurring at a more distantly located kinase domain within the holoenzyme rather than an adjacent one, thereby considering the holoenzyme to be a "coincidence detector" for Ca^{2+}/CaM binding. This model is consistent with experiments that show noncooperative acquisition of substrate-directed kinase activity as
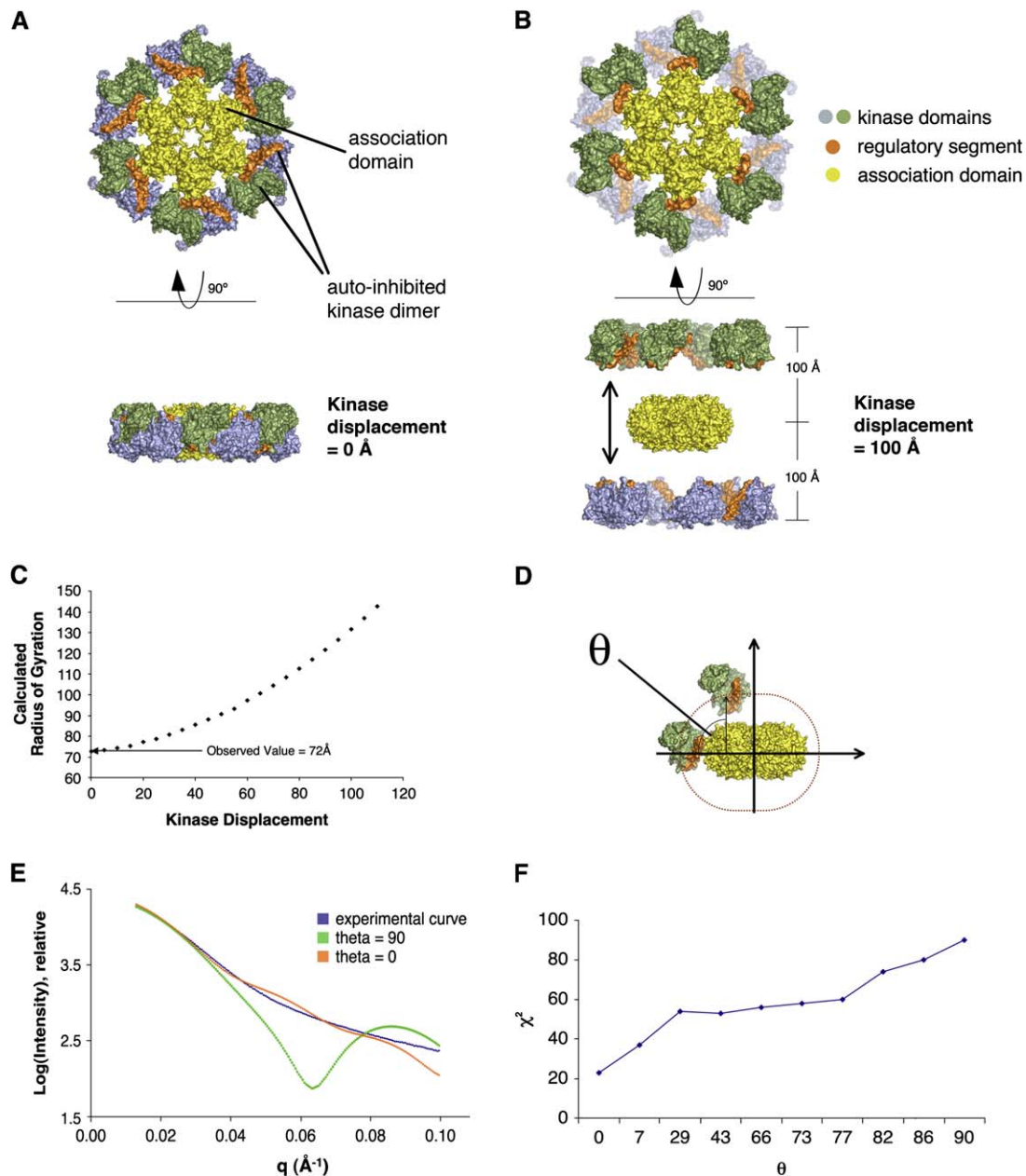
Figure 5. Rigid-Body Modeling Scheme for SAXS Analysis

Six autoinhibited kinase-domain dimers were placed around a central association domain as described in the text. The kinases were separated from one another in steps of 5 Å (this variable was defined as "kinase displacement") and the theoretical solution X-ray scattering was calculated for each resulting model.

(A) A value of kinase displacement equal to 0 Å, corresponding to a model where the autoinhibited kinase domains are in the dimer seen in the crystal structure. The resulting model is a disc with a diameter of ~200 Å and a height of ~60 Å.

(B) A value of kinase displacement equal to 100 Å resulting in a model with diameter of ~200 Å and a height of ~200 Å.

(C) As the value of kinase displacement increases, the calculated R_g diverges sharply from the experimental value of ~72 Å.

(D) The rings of autoinhibited kinase domains were moved above and below the association domains while simultaneously shrinking the radius of the kinase rings to generate a series of models with essentially equivalent R_g values (matched to the experimental value). The different models can all be described by a single variable, θ, that represents the angle between the midplane of the association domain and a vector connecting the center of an association-domain dimer and the center of mass of the autoinhibited kinase domain.

(E) Theoretical X-ray scattering curves were calculated for models corresponding to different values of θ. At a value of θ equal to 0, corresponding to a model in which the individual autoinhibited kinase domains are held together as dimer pairs in an outer ring that is coplanar with the central plane, the curve approximates the actual data much better. This is quantified in (F) where the χ^2 statistic calculated by the program Crysol (Svergun et al., 1995), which compares the calculated scattering curve to the experimental one, is optimal at $\theta = 0$.
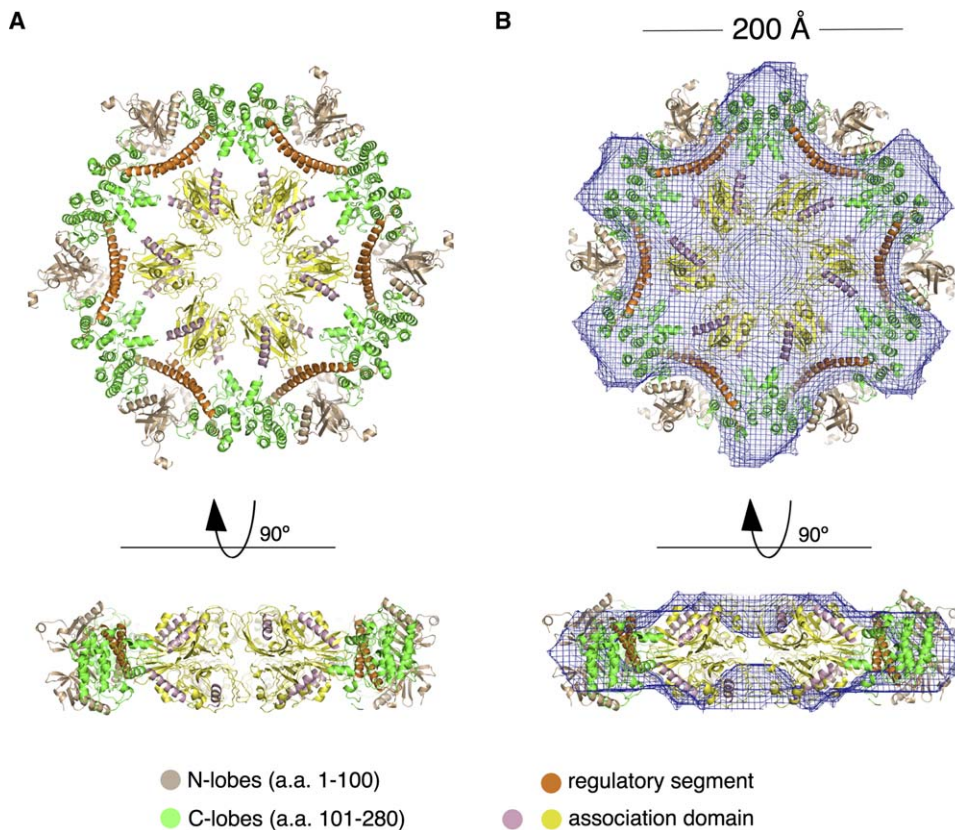
Figure 6. Ab-Initio Shape Restorations using SAXS from CaMKII

(A) The holoenzyme model that resulted from the rigid body modeling described above. In green are the more electron-dense C lobes of the kinases and in beige are the N lobes of the kinases.

(B) Shown in blue mesh is the SAXS shape reconstruction. The model shown in (A) was fit into the SAXS shape reconstruction as described in the Experimental Procedures.

a function of CaM concentration (Bradshaw et al., 2003). On the other hand, we show here that Ca^{2+}/CaM binds to the CaMKII holoenzyme with an apparent Hill coefficient of ∼2 (see also Gaertner et al. [2004]). If the dimer is the fundamental unit of the holoenzyme assembly, it is very likely that once Ca^{2+}/CaM has bound to one autoinhibited kinase domain, the next binding event will occur within the same dimer pair and not at a more distantly located one. Such a process, if unconstrained, would generate pairs of activated kinase domains that would be free to phosphorylate each other immediately.

We have considered whether there are elements to the structure of the holoenzyme that may bring about a delay in transautophosphorylation after the initial binding of Ca^{2+}/CaM. If Ca^{2+}/CaM binding were to separate the two kinase domains in a dimer pair above and below the midplane of the association domains, as suggested by some of the electron microscopic reconstructions (Kolodziej et al., 2000), then transphosphorylation might require adjacent kinase dimers to be activated, so that kinase domains located on the same side of the midplane can reach each other. This kind of mechanism might enable the holoenzyme to serve as a coincidence detector as proposed by Schulman and co-

workers, even though two Ca^{2+}/CaM bind cooperatively to each kinase dimer.

The connection between the helical regulatory segment of the kinase domain and the first helix of the association domain is almost certainly flexible, as indicated by the sequence and by the location of alternative splice sites at this junction (Figure S1). The outer surface of the association domain, which is mainly negatively charged, has a localized region of positive charge located alongside the edge of the N-terminal α helix of the association domain (Figure 7B, inset). The residues that form this positively charged patch (Arg 371, Arg 453, and Arg 461 in the *C. elegans* CaMKII association domain) are conserved (Figure S1). The linker segment that leads into the N-terminal α helix of the association domain contains 3 to 4 acidic residues that are also conserved (Figure S1). These residues are either disordered or have variable structure in the association domains and serve no obvious structural function.

We speculate that this negatively charged linker region could fold back onto the surface of the association domain when the kinase is activated and thereby interact with the positively charged patch, which is located close to the connection point of the linker. Such an interaction would result in
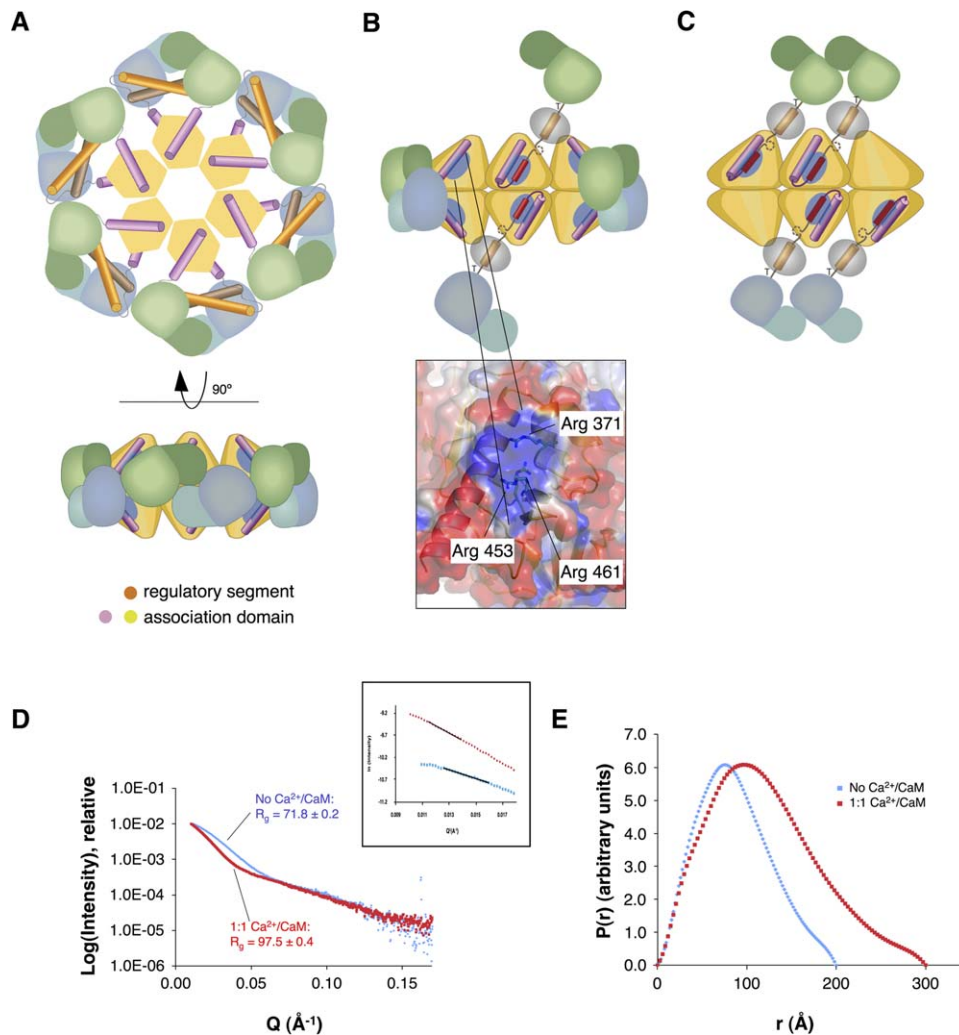
Figure 7. Speculation Regarding the Activation of CaMKII by Ca^{2+}/CaM

(A) A schematic diagram of the holoenzyme in its fully autoinhibited form.

(B) Ca^{2+}/CaM binds to a regulatory segment of a kinase dimer, releasing the other regulatory segment to bind a second Ca^{2+}/CaM. Release of the dimer pair reveals a basic patch, shown inset with the electrostatic surface overlaid on the structure. This basic patch may then interact with an acidic region on the linker, directing the kinase domains above and below the midplane of the association domain.

(C) When an adjacent autoinhibited kinase dimer binds to two Ca^{2+}/CaM, the kinase domains will again be directed above and below the midplane. They will now encounter the previously activated kinase domains, and transphosphorylation of Thr 286 can occur.

(D) The addition of Ca^{2+}/CaM to CaMKII causes a change in the shape of the solution SAXS curve. The intensity of the curve without Ca^{2+}/CaM was multiplied by 1.7 so as to overlay the graphs. The Guinier region, shown as an inset, is linear for both curves in a region of $s*R_g = .9 - 1.3$. By fitting the Guinier equation (with the program PRIMUS), the value of R_g was determined to be 71.8 ± 0.2 without Ca^{2+}/CaM and 97.5 ± 0.4 when Ca^{2+}/CaM is added. The presence of the linear Guinier region in the $s*R_g$ region < 1.3 indicates that the samples are not aggregated.

(E) The P(r) function, as calculated by the program GNOM (Svergun, 1992), for CaMKII with and without the addition of Ca^{2+}/CaM.

the separation of the two kinase domains from a dimer pair above and below the midplane of the association domain upon activation (Figure 7B). Such separation of adjacent kinase domains would generate an activated holoenzyme assembly that bears similarity to the electron microscopic reconstructions of Waxham and coworkers (Gaertner et al., 2004), as shown schematically (Figure 7C).

SAXS data for mouse CaMKIIα holoenzyme measured in the presence and absence of Ca^{2+}/CaM show that the radius of gyration increases from 72.15 ± 0.06 Å (maximum diameter of 235 Å) to 90.48 ± 0.06 Å (maximum diameter of 260 Å) upon the addition of Ca^{2+}/CaM (Figures 7D and 7E). We interpret the ~18 Å increase in the radius of gyration upon the addition of Ca^{2+}/CaM to represent the release of the kinase domains from the dimeric assembly and their movement away from the centrally docked positions. These results do not allow us to build a meaningful model of the activated state of the holoenzyme, but such a dramatic change in conformation may have an effect on the binding of the many proteins that interact with CaMKII in the postsynaptic density.

Conclusions

Our structure of the autoinhibited kinase domain of CaMKII is quite different from those of monomeric Ca^{2+}/CaM-activated enzymes, and one unexpected aspect is the formation of a dimeric coiled-coil strut by the CaM-responsive regulatory segments. The architecture of the dimer is such that the intrinsically active kinase domains are held apart in a way that requires Ca^{2+}/CaM for transphosphorylation and the acquisition of "memory." The organization of the dimer most likely reflects an evolutionary solution to the problem of preventing accidental transautophosphorylation despite the high concentration of kinase domains in the holoenzyme, ensuring that the activity of this signaling device responds appropriately to Ca^{2+} levels.

A model for the holoenzyme in which the kinase domains are arranged in a ring that is coplanar with the central hub is consistent with our SAXS and X-ray diffraction data. The model suggests that the kinase domains are inhibited cooperatively, and we present data for the binding of Ca^{2+}/CaM to the holoenzyme that is consistent with this. A separation of the kinase domains above and below the midplane of the assembly after the activation of a dimer may provide a mechanism for delaying the onset of transautophosphorylation until an adjacent dimer is activated, and this has interesting consequences for the mechanism by which CaMKII can sense the frequency of Ca^{2+} pulses.

The results presented here add to the evidence that CaMKII holoenzyme is an intricately controlled signaling switch that can respond in a concerted manner to stimulation by Ca^{2+}. We await further high-resolution analysis of the holoenzyme assembly, which will reveal the precise connections between the association domains and the autoinhibited kinase domains that allow the molecule to develop a chemical memory that depends on the temporal properties of the Ca^{2+} stimulus.

EXPERIMENTAL PROCEDURES

Protein Expression and Purification

DNA encoding residues 1–340 of *C. elegans* CaMKII (*unc-43*) was subcloned into pET-28 (Novagen) modified to contain a PreScission Protease (Pharmacia) site between the N-terminal 6-histidine tag and the coding sequence. Aspartate 135 was mutated to Asparagine (QuikChange mutagenesis kit, Stratagene). Protein expression was induced in BL21(DE3) strain *E. coli* with 0.4 mM IPTG for 12 hr at 18°. The cells were lysed using a French Press, and the cellular debris was removed by centrifugation at 100,000 × g for 1 hr. The CaMKII fragment was purified with a 5 ml HiTrap HisBind column (Pharmacia) and then the N-terminal 6-histidine tag was cleaved using PreScission Protease according to the manufacturer's directions (Pharmacia). The protein was further purified with SP ion exchange and S200 size exclusion chromatography. The buffer from the gel filtration was 20 mM Tris (pH 8.0), 150 mM KCl, and 1 mM DTT. DNA encoding full-length *C. elegans* CaMKII was subcloned into pFastBac-1 (Gibco). Aspartate 135 was mutated to Asparagine as above. Recombinant bacmid DNA was prepared according to the manufacturer's instructions (Bac-to-Bac expression system, Gibco, BRL) and transfected into Sf9 cells. Baculovirus obtained from the transfection was used to infect Sf9 cells grown in suspension to a density of 2.5 × 10⁶ per ml at a multiplicity of infection of approximately 10. Cells were grown for 48 hr, centrifuged, and resuspended in 50 mM HEPES (pH 7.4), 50 mM KCl, and 10% glycerol. Cells (4L) were lysed with a French Press and centri-

fuged at 100,000 × g to remove cellular debris. The protein was purified with SP, Q, and size-exclusion chromatography. The final buffer from the gel filtration was 20 mM Tris (pH 8.0), 150 mM KCl, 1 mM DTT.

DNA encoding full-length *M. musculus* CaMKIIα was subcloned into a pFastBac-1 plasmid modified to contain a C-terminal, 6-histidine tag. Aspartate 135 was mutated to Asparagine as above. The protein was expressed and purified as described for the *C. elegans* full-length protein except that an additional nickel affinity column was added after the SP column. The final buffer from the gel filtration was 20 mM Tris (pH 8.3), 200 mM KCl, 5% glycerol.

Gallus gallus CaM was expressed using a pET-15b vector. Lysine 75 was mutated to Cysteine as above. Purification and labeling with IAEDANS fluorophore were performed as described (Putkey and Waxham, 1996).

The association domain of *M. musculus* CaMKIIα (residues 336–478) was expressed and purified as described (Hoelz et al., 2003).

Crystallization and Structure Determination

The *C. elegans* autoinhibited kinase domain was concentrated to 1.03 mM and mixed with an equal amount of 1.6 M sodium malonate (pH 7.0) on a coverslip. 1.5% 1,2,3-heptanetriol was added directly to the drop, and the drop was equilibrated with a reservoir of 1.6 M sodium malonate. The crystals (space group P2₁; a = 46.1 Å, b = 77.1 Å, c = 119.5 Å, β = 96.7°) grew to their full size of 0.100 × 0.200 × 0.40 mm³ within 24 hr. The crystals were transferred to 1.6 M sodium malonate, 20% glycerol, and then flash frozen in liquid nitrogen and used for X-ray data collection (Advanced Light Source [ALS], Beamline 8.2.2). X-ray data were processed using HKL2000 (Otwinowski and Minor, 1997). The structure was solved by molecular replacement using Phaser (McCoy et al., 2005), with phosphorylase kinase (2phk) as the search model (Lowe et al., 1997). All models were refined using the programs CNS (Brunger et al., 1998) and O (Kleywegt and Jones, 1996). The final structure was refined to 1.8 Å resolution (R_free and R_working are 0.236 and 0.216, respectively; Table S1). The model consists of residues 5 to 315 and 9 to 318 in molecules A and B, respectively, and 447 water molecules.

Structural figures were prepared with the program PyMOL (DeLano, 2002). Maps of electrostatic surfaces were calculated using GRASP (Nicholls et al., 1991).

Molecular Dynamics

Molecular dynamics simulations were carried out using periodic boundary conditions with a truncated octahedral geometry and water extending a minimum of 10 Å beyond the protein. The net charge on the dimer system was neutralized by the addition of 5 Cl⁻ ions. The kinase with regulatory segment was neutralized by addition of 2 Cl⁻ ions. The kinase without the regulatory segment was neutralized by the addition of 4 K⁺ ions. The simulations were carried out using the Sander module of AMBER 8.0 (Case et al., 2004, University of California, San Francisco) using 10 xeon processors on an IBM X series 345 cluster, essentially as described for the Src kinases (Young et al., 2001).

Binding Experiments

The binding experiments were carried out as described by Waxham and coworkers (Gaertner et al., 2004) using a Spex Jobin Yvon FluoroMax-3 fluorometer with a Peltier-temperature controlled sample chamber at 25°C. Excitation and emission slit bandpass was set at 5 nm. We noted marked photobleaching during the course of the experiment and corrected for this empirically. All curves were measured in triplicate. The data were normalized such that maximal binding for each experiment was equal to 1. The binding curves were plotted and analyzed using the program Prism (version 4, GraphPad Software). The data was fit to the Hill equation

$$Y = Y_{min} + \frac{(Y_{max} - Y_{min})}{1 + \left(\frac{10^{(LogEC_{50})}}{10^{[L]}}\right)^n},$$

where Y is the fraction bound as measured by relative fluorescence intensity, EC_{50} is the concentration at half maximal binding, [L] is the log of the concentration of kinase, and n is the apparent Hill coefficient.

Small-Angle X-Ray Scattering (SAXS)

SAXS data for the CaM binding experiments and the *M. musculus* holoenzyme shape reconstruction were measured at the BESSRC-CAT beamline (12-IDC) at the Advanced Photon Source (APS) as described (Davies et al., 2005). SAXS data for the rigid body modeling and the shape reconstructions of the *C. elegans* holoenzyme were collected at the SIBYLS beamline at ALS using a Mar 165 CCD area detector (165 mm diameter). A 15 μl sample was placed in a 1 mm thick chamber with two windows of 25 μm Mica. The detector to sample distance was 1.5 m. A single-crystal monochromator was used with an energy of 10 keV ($\lambda = 1.298$ Å). The curves were measured at concentrations of 35 mg/ml, 17.5 mg/ml, and 8.25 mg/ml, and there was no evidence for aggregation at higher concentrations. The R_g was approximated using PRIMUS (Kovnarev et al., 2003) to evaluate the Guinier equation and GNOM (Svergun, 1992) to evaluate the P(r) function. The value of the maximum diameter of the particle, D_{max}, was determined empirically by examining the quality of the fit to the experimental data for a range of D_{max} values. The R_g given by both methods was in good agreement, although dependent on the choice of the initial parameters (in both cases). A consensus value of 72 Å was used in the rigid body modeling.

For the CaM binding experiments, the mouse holoenzyme was diluted to 35 μM in 200 mM Tris (pH 8), 200 mM KCl, 2 mM $CaCl_2$, and 5% glycerol. The protein was divided into two samples; to one was added 35 μM CaM and to the other was added an equivalent amount of buffer. Five 1 s exposures were taken for each sample and for the buffer control.

Structures for the rigid body modeling of the SAXS data were generated using the program PyMOL. The R_g value for each model was calculated using the program package Crysol (Svergun et al., 1995) and compared to the experimentally determined scattering curve for the *C. elegans* holoenzyme construct for Q values between 0.01039 and 0.2612 Å^{-1}.

Shape reconstructions were done with the program DAMMIN (Svergun, 1999) using the default settings in the "slow" annealing mode using a Q range of 0.0155 to 0.1599 Å^{-1} for the *C. elegans* reconstruction, 0.0098 and 0.2072 Å^{-1} for the *M. musculus* reconstruction, and 0.0241 to 0.2772 Å^{-1} in the association-domain reconstructions. The dummy atom models resulting from ten individual DAMMIN runs were aligned, averaged, and scored with a normalized structural difference (NSD) using the program package DAMAVER (Volkov and Svergun, 2003). Models with a large NSD were rejected. The resulting probability map was filtered to a most probable structure using DAMFILT (Volkov and Svergun, 2003). The 6-fold model of the association domain was fit into the filtered model using the program package SITUS (Wriggers et al., 1999). This structure was then used as a guide to fit the model determined by rigid body modeling into the shape reconstruction.

Supplemental Data

Supplemental Data include seven figures and one table and can be found with this article online at http://www.cell.com/cgi/content/full/123/5/849/DC1/.

REFERENCES

Bradshaw, J.M., Hudmon, A., and Schulman, H. (2002). Chemical quenched flow kinetic studies indicate an intraholoenzyme autophosphorylation mechanism for Ca2+/calmodulin-dependent protein kinase II. J. Biol. Chem. *277*, 20991–20998.

Bradshaw, J.M., Kubota, Y., Meyer, T., and Schulman, H. (2003). An ultrasensitive Ca2+/calmodulin-dependent protein kinase II-protein phosphatase 1 switch facilitates specificity in postsynaptic calcium signaling. Proc. Natl. Acad. Sci. USA *100*, 10512–10517.

Brickey, D.A., Bann, J.G., Fong, Y.L., Perrino, L., Brennan, R.G., and Soderling, T.R. (1994). Mutational analysis of the autoinhibitory domain of calmodulin kinase II. J. Biol. Chem. *269*, 29047–29054.

Brunger, A.T., Adams, P.D., Clore, G.M., DeLano, W.L., Gros, P., Grosse-Kunstleve, R.W., Jiang, J.S., Kuszewski, J., Nilges, M., Pannu, N.S., et al. (1998). Crystallography & NMR system: a new software suite for macromolecular structure determination. Acta Crystallogr. D Biol. Crystallogr. *54*, 905–921.

Case, D.A., Darden, T.A., Cheatham, I.T.E., Simmerling, C.L., Wang, J., Duke, R.E., Luo, R., Merz, K.M., Wang, B., Pearlman, D.A., et al. (2004). AMBER (computer program). University of California San Francisco.

Colbran, R.J. (1993). Inactivation of Ca2+/calmodulin-dependent protein kinase II by basal autophosphorylation. J. Biol. Chem. *268*, 7163–7170.

Crick, F. (1953). The packing of [alpha]-helices: simple coiled-coils. Acta Crystallogr. *6*, 689–697.

Davies, J.M., Tsuruta, H., May, A.P., and Weis, W.I. (2005). Conformational changes of p97 during nucleotide hydrolysis determined by small-angle X-Ray scattering. Structure (Camb) *13*, 183–195.

De Koninck, P., and Schulman, H. (1998). Sensitivity of CaM kinase II to the frequency of Ca2+ oscillations. Science *279*, 227–230.

DeLano, W.L. (2002). The PyMOL Molecular Graphics System (San Carlos, CA: DeLano Scientific).

Gaertner, T.R., Kolodziej, S.J., Wang, D., Kobayashi, R., Koomen, J.M., Stoops, J.K., and Waxham, M.N. (2004). Comparative analyses of the three-dimensional structures and enzymatic properties of alpha, beta, gamma and delta isoforms of Ca2+-calmodulin-dependent protein kinase II. J. Biol. Chem. *279*, 12484–12494.

Goldberg, J., Nairn, A.C., and Kuriyan, J. (1996). Structural basis for the autoinhibition of calcium/calmodulin-dependent protein kinase I. Cell *84*, 875–887.

Hanson, P.I., and Schulman, H. (1992). Inhibitory autophosphorylation of multifunctional Ca2+/calmodulin-dependent protein kinase analyzed by site-directed mutagenesis. J. Biol. Chem. *267*, 17216–17224.

Hanson, P.I., Meyer, T., Stryer, L., and Schulman, H. (1994). Dual role of calmodulin in autophosphorylation of multifunctional CaM kinase may underlie decoding of calcium signals. Neuron *12*, 943–956.

Hoelz, A., Nairn, A.C., and Kuriyan, J. (2003). Crystal structure of a tetradecameric assembly of the association domain of Ca2+/calmodulin-dependent kinase II. Mol. Cell *11*, 1241–1251.

Hu, S.H., Parker, M.W., Lei, J.Y., Wilce, M.C., Benian, G.M., and Kemp, B.E. (1994). Insights into autoregulation from the crystal structure of twitchin kinase. Nature *369*, 581–584.

Huang, C.Y., Yuan, C.J., Blumenthal, D.K., and Graves, D.J. (1995). Identification of the substrate and pseudosubstrate binding sites of phosphorylase kinase gamma-subunit. J. Biol. Chem. *270*, 7183–7188.

Hudmon, A., and Schulman, H. (2002). Structure-function of the multifunctional Ca2+/calmodulin-dependent protein kinase II. Biochem. J. *364*, 593–611.

King, M.M., Shell, D.J., and Kwiatkowski, A.P. (1988). Affinity labeling of the ATP-binding site of type II calmodulin-dependent protein kinase by 5′-p-fluorosulfonylbenzoyl adenosine. Arch. Biochem. Biophys. *267*, 467–473.

Kleywegt, G.J., and Jones, T.A. (1996). Efficient rebuilding of protein structures. Acta Crystallogr. D Biol. Crystallogr. *52*, 829–832.

Kolodziej, S.J., Hudmon, A., Waxham, M.N., and Stoops, J.K. (2000). Three-dimensional reconstructions of calcium/calmodulin-dependent (CaM) kinase IIalpha and truncated CaM kinase IIalpha reveal a unique organization for its structural core and functional domains. J. Biol. Chem. *275*, 14354–14359.

Kovnarev, P.V., Volkov, A.V., Sokolova, A.V., Koch, M.H.J., and Svergun, D.I. (2003). PRIMUS: a Windows PC-based system for small-angle scattering data analysis. J. Appl. Cryst. *36*, 1277–1282.

Lai, Y., Nairn, A.C., and Greengard, P. (1986). Autophosphorylation reversibly regulates the Ca2+/calmodulin-dependence of Ca2+/calmodulin-dependent protein kinase II. Proc. Natl. Acad. Sci. USA *83*, 4253–4257.

Lisman, J., Schulman, H., and Cline, H. (2002). The molecular basis of CaMKII function in synaptic and behavioural memory. Nat. Rev. Neurosci. *3*, 175–190.

Lou, L.L., and Schulman, H. (1989). Distinct autophosphorylation sites sequentially produce autonomy and inhibition of the multifunctional Ca2+/calmodulin-dependent protein kinase. J. Neurosci. *9*, 2020–2032.

Lowe, E.D., Noble, M.E., Skamnaki, V.T., Oikonomakos, N.G., Owen, D.J., and Johnson, L.N. (1997). The crystal structure of a phosphorylase kinase peptide substrate complex: kinase substrate recognition. EMBO J. *16*, 6646–6658.

Lu, C.S., Hodge, J.J., Mehren, J., Sun, X.X., and Griffith, L.C. (2003). Regulation of the Ca2+/CaM-responsive pool of CaMKII by scaffold-dependent autophosphorylation. Neuron *40*, 1185–1197.

Lupas, A., Van Dyke, M., and Stock, J. (1991). Predicting coiled coils from protein sequences. Science *252*, 1162–1164.

Mayans, O., van der Ven, P.F., Wilm, M., Mues, A., Young, P., Furst, D.O., Wilmanns, M., and Gautel, M. (1998). Structural basis for activation of the titin kinase domain during myofibrillogenesis. Nature *395*, 863–869.

McCoy, A.J., Grosse-Kunstleve, R.W., Storoni, L.C., and Read, R.J. (2005). Likelihood-enhanced fast translation functions. Acta Crystallogr. D Biol. Crystallogr. *61*, 458–464.

Meador, W.E., Means, A.R., and Quiocho, F.A. (1993). Modulation of calmodulin plasticity in molecular recognition on the basis of x-ray structures. Science *262*, 1718–1721.

Meyer, T., Hanson, P.I., Stryer, L., and Schulman, H. (1992). Calmodulin trapping by calcium-calmodulin-dependent protein kinase. Science *256*, 1199–1202.

Miller, S.G., and Kennedy, M.B. (1986). Regulation of brain type II Ca2+/calmodulin-dependent protein kinase by autophosphorylation: A Ca2+-triggered molecular switch. Cell *44*, 861–870.

Miller, S.G., Patton, B.L., and Kennedy, M.B. (1988). Sequences of autophosphorylation sites in neuronal type II CaM kinase that control Ca2(+)-independent activity. Neuron *1*, 593–604.

Morris, E.P., and Torok, K. (2001). Oligomeric structure of alpha-calmodulin-dependent protein kinase II. J. Mol. Biol. *308*, 1–8.

Nelson, A.B., Gittis, A.H., and du Lac, S. (2005). Decreases in CaMKII activity trigger persistent potentiation of intrinsic excitability in spontaneously firing vestibular nucleus neurons. Neuron *46*, 623–631.

Nicholls, A., Sharp, K.A., and Honig, B. (1991). Protein folding and association: insights from the interfacial and thermodynamic properties of hydrocarbons. Proteins *11*, 281–296.

Nolen, B., Taylor, S., and Ghosh, G. (2004). Regulation of protein kinases: Controlling activity through activation segment conformation. Mol. Cell *15*, 661–675.

Otwinowski, Z., and Minor, W. (1997). Processing of X-ray diffraction data collected in oscillation mode. Methods Enzymol. *276*, 307–326.

Putkey, J.A., and Waxham, M.N. (1996). A peptide model for calmodulin trapping by calcium/calmodulin-dependent protein kinase II. J. Biol. Chem. *271*, 29619–29623.

Rich, R.C., and Schulman, H. (1998). Substrate-directed function of calmodulin in autophosphorylation of Ca2+/calmodulin-dependent protein kinase II. J. Biol. Chem. *273*, 28424–28429.

Schworer, C.M., Colbran, R.J., Keefer, J.R., and Soderling, T.R. (1988). Ca2+/calmodulin-dependent protein kinase II. Identification of a regulatory autophosphorylation site adjacent to the inhibitory and calmodulin-binding domains. J. Biol. Chem. *263*, 13486–13489.

Shields, S.M., Vernon, P.J., and Kelly, P.T. (1984). Autophosphorylation of calmodulin-kinase II in synaptic junctions modulates endogenous kinase activity. J. Neurochem. *43*, 1599–1609.

Smith, M.K., Colbran, R.J., Brickey, D.A., and Soderling, T.R. (1992). Functional determinants in the autoinhibitory domain of calcium/calmodulin-dependent protein kinase II. Role of His282 and multiple basic residues. J. Biol. Chem. *267*, 1761–1768.

Svergun, D.I. (1992). Determination of the regularization parameter in indirect-transform methods using perceptual criteria. J. Appl. Crystallogr. *25*, 495–503.

Svergun, D.I. (1999). Restoring low resolution structure of biological macromolecules from solution scattering using simulated annealing. Biophys. J. *76*, 2879–2886.

Svergun, D.I., Barberato, C., and Koch, M.H.J. (1995). Crysol—a program to evaluate X-ray solution scattering of biological macromolecules from atomic coordinates. J. Appl. Crystallogr. *28*, 768–773.

Thiel, G., Czernik, A.J., Gorelick, F., Nairn, A.C., and Greengard, P. (1988). Ca2+/calmodulin-dependent protein kinase II: identification of threonine-286 as the autophosphorylation site in the alpha subunit associated with the generation of Ca2+-independent activity. Proc. Natl. Acad. Sci. USA *85*, 6337–6341.

Volkov, A.V., and Svergun, D.I. (2003). Uniqueness of ab initio shape determination in small-angle scattering. J. Appl. Crystallogr. *36*, 860–864.

Walshaw, J., and Woolfson, D.N. (2001). Socket: a program for identifying and analysing coiled-coil motifs within protein structures. J. Mol. Biol. *307*, 1427–1450.

Woodgett, J.R., Davison, M.T., and Cohen, P. (1983). The calmodulin-dependent glycogen synthase kinase from rabbit skeletal muscle. Purification, subunit structure and substrate specificity. Eur. J. Biochem. *136*, 481–487.

Wriggers, W., Milligan, R.A., and McCammon, J.A. (1999). Situs: A package for docking crystal structures into low-resolution maps from electron microscopy. J. Struct. Biol. *125*, 185–195.

Yang, E., and Schulman, H. (1999). Structural examination of autoregulation of multifunctional calcium/calmodulin-dependent protein kinase II. J. Biol. Chem. *274*, 26199–26208.

Young, M.A., Gonfloni, S., Superti-Furga, G., Roux, B., and Kuriyan, J. (2001). Dynamic coupling between the SH2 and SH3 domains of c-Src and Hck underlies their inactivation by C-terminal tyrosine phosphorylation. Cell *105*, 115–126.

Accession Numbers

The coordinates for the crystal structure of the autoinhibited kinase domain from *C. elegans* CaMKII is deposited in the Protein Data Bank with the ID 2BDW. Please note that the numbering of the residues in the PDB file has been changed so that it corresponds to the numbering in the mouse CaMKIIα isoform.